# Facile synthesis of $Li_{1.2}Ni_{0.13}Co_{0.13}Mn_{0.54}O_2$ by a thermal decomposition of eutectic Li-Ni-Co-Mn acetate as lithium ion battery cathodes

*Xiaoling Lang, Chenhao Zhao*[*]*, Zhibiao Hu, TianFu Huang, Kaiyu Liu*

College of Chemistry & Materials Science, LongYan University, Fujian LongYan 364012, China
[*]E-mail: zhaochenhao123456@163.com

Lithium rich layered oxide $Li_{1.2}Ni_{0.13}Co_{0.13}Mn_{0.54}O_2$ have been successfully prepared by a simple decomposition of eutectic Li-Ni-Co-Mn acetate without using any solvent or additive. The influences of calcination temperatures on the structures and electrochemical performances of $Li_{1.2}Ni_{0.13}Co_{0.13}Mn_{0.54}O_2$ are clearly studied, and the results indicate that the increased temperature helps to improve the layered structure and particle size. At an optimal calcination temperature of $850^oC$, the resultant nanoparticles present the size of ~200 nm. As lithium ion battery cathodes, the $850^oC$ sample has an initial discharge capacity of 264.9 mAh $g^{-1}$ with Coulombic efficiency of 80.1% at 20 mA $g^{-1}$ and stable discharge capacity of 140.1 mAh $g^{-1}$ at 600 mA $g^{-1}$. Besides, it also can retain a capacity value of 203.0 mAh $g^{-1}$ at 100 mA $g^{-1}$ after 50 cycles. Anyway, the eutectic Li-Ni-Co-Mn acetate route is suitable for the synthesis of lithium rich layered oxides.

## 1. INTRODUCTION

To meet the increasing requirement of lithium ion battery with high discharge capacity, high energy density and good cycling stability, the development of advanced cathode materials needto be intensively carried out. [1-3]. At present, a type of lithium rich layered oxides (LLOs), generally described as a chemical formula of $xLi_2MnO_3·(1-x)LiMO_2$ (M = Mn, Co, Cr, Fe, $Ni_{1/2}Mn_{1/2}$, $Ni_{1/3}Co_{1/3}Mn_{1/3}$, etc.) has attracted much more attentions due to their high discharge capacity ($>$230 mAh $g^{-1}$) compared with commercial $LiFePO_4$, $LiMn_2O_4$ and $LiCoO_2$ [4-7]. In fact, when $xLi_2MnO_3·(1-x)LiMO_2$ electrodes are charged to 4.6 V or higher, the $Li_2MnO_3$ component can be activated and simultaneously transformed into another active component layered $MnO_2$, resulting in

high discharge capacity nature of lithium-rich layered oxides [8-10]. On the other hand, the $Li_2MnO_3$ and resultant layered $MnO_2$ can be treated as a structural stabilizer to improve cycling stability of the other $LiMO_2$ phase during cycling especially at wide voltage widow (e. g., 4.8 V) [11].

Among all lithium-rich layered oxides, the $0.5Li_2MnO_3 \cdot 0.5LiNi_{1/3}Co_{1/3}Mn_{1/3}O_2$ ($Li_{1.2}Ni_{0.13}Co_{0.13}Mn_{0.54}O_2$) has been widely studied because of its high discharge capacity, moderate cycling performance and good rate capability. The improved electrochemical performances of $Li_{1.2}Ni_{0.13}Co_{0.13}Mn_{0.54}O_2$ can be ascribed to the good synergistic effect of $Li_2MnO_3$ and $LiNi_{1/3}Co_{1/3}Mn_{1/3}O_2$ components and the appropriate co-existence of Co element [12-14]. So far, Conventional preparation methods including sol–gel [15, 16], co-precipitation [17-19], solid state [20], solution combustion [21], molten salt [22, 23], and polymer gel [24] routes have been successfully used to prepare this promising $Li_{1.2}Ni_{0.13}Co_{0.13}Mn_{0.54}O_2$, showing the structural and electrochemical properties of $Li_{1.2}Ni_{0.13}Co_{0.13}Mn_{0.54}O_2$ can be depended upon different synthesis methods and preparation conditions [25].

During the preparation of some metal oxides such as $Li_{1.2}Ni_{0.13}Co_{0.13}Mn_{0.54}O_2$, it is still a challenge that uniform mixing of raw materials (i.e., Li, Ni, Co and Mn metal ions), especially at the atomic level during the preparation of lithium rich layered oxides [26, 27]. Consideration of the low melting point of metal acetate (i.e., $Mn(AC)_2 \cdot 4H_2O$: ~80$^o$C, $Co(AC)_2 \cdot 4H_2O$: ~140$^o$C, $Ni(AC)_2 \cdot 4H_2O$: ~115$^o$C, $Li(AC) \cdot 2H_2O$: ~70$^o$C)，eutectic acetate with a state of viscous solution may be obtained by heating the acetate mixture in a suitable temperature (80-120$^o$C), and formed eutectic state should be helpful for the uniform mixing of precursor. Aroused by the fact that eutectic acetate route has been used to prepare multi-component metal oxide such as spinel $LiNi_{1/2}Mn_{3/2}O_4$ [28, 29] and others [30]. Herein, we develop a facile thermal decomposition of eutectic Li-Ni-Co-Mn acetate to prepare lithium rich layered oxide $Li_{1.2}Ni_{0.13}Co_{0.13}Mn_{0.54}O_2$ samples [15-19]. Mainly, the influences of calcination temperatures on the structural and electrochemical properties of target products are investigated and discussed in the text.

## 2. EXPERIMENTAL

### 2.1 Synthesis of $Li_{1.2}Ni_{0.13}Co_{0.13}Mn_{0.54}O_2$:

All the reagents are of analytical grade and were used without purification. $Li_{1.2}Ni_{0.13}Co_{0.13}Mn_{0.54}O_2$(the stoichiometric number is determined by added raw materials) samples were prepared by a facile eutectic Li-Ni-Co-Mn acetate route, described as follow: 1.3235 g of $Mn(AC)_2 \cdot 4H_2O$, 0.3238 g of $Co(AC)_2 \cdot 4H_2O$, 0.3236 g of $Ni(AC)_2 \cdot 4H_2O$ and 1.260 g of $Li(AC) \cdot 2H_2O$ were placed in an agate mortar, and ground for about 10 min to form solid mixture. The resulting mixture is transformed into a reagent bottom, and kept at 100$^o$C for 1 h to form eutectic Li-Ni-Co-Mn acetate with a state of viscous solution. After solidification, the obtained "gel"-like product was decomposed at 450$^o$C for 4 h, ground uniformly, and then was sintered at a temperature of 750, 850 or 950$^o$C for 10 h under air, cooled naturally to room temperature.

*2.2 Structural characterization:*

X-ray diffraction (XRD) patterns were performed at the scanning rate of $0.04^o$/s within $2\theta$ degree of 20-80$^o$ using a Rigaku D/max-2400 powder X-ray diffractometer with Cu-K$\alpha$ radiation. Scanning electron microscopy (SEM; JEOL JSM-6700F) images were collected to characterize the morphologies and sizes of obtained samples.

*2.3 Electrochemical characterization:*

The electrochemical experiments were performed using coin cells (CR 2032) at about 30$^o$C. The working electrodes were prepared as the following: after mixing of $Li_{1.2}Ni_{0.13}Co_{0.13}Mn_{0.54}O_2$, binder poly(vinyl difluoride) (PVDF), and acetylene black at a weight ratio of 8 : 1 : 1, the resulting mixtures were slurried with N-methyl-2-pyrrolidone (NMP), pasted onto aluminum foils, dried at 80$^o$C for 5 h, and cut into discs with a diameter of 12 mm. The working electrode possessed a loading density of 2.6±0.6 mg cm$^{-2}$. Polymers (Celgard) and commercial LBC 305-01 LiPF$_6$ solution (Shenzhen Xinzhoubang) were used as separators and electrolyte, respectively. The cells were assembled in an argon-filled glove box. Galvanostatic cycling tests were conducted on a Land CT2001A battery system at various current rates (1 C = 200 mA g$^{-1}$) between 2.0 and 4.7 V. Cyclic voltammetric (CV) behaviors were performed on a LK 2005A Electrochemical Workstation at a scanning rate of 0.1 mV s$^{-1}$ within 2.0-4.8 V.

## 3. RESULTS AND DISCUSSION
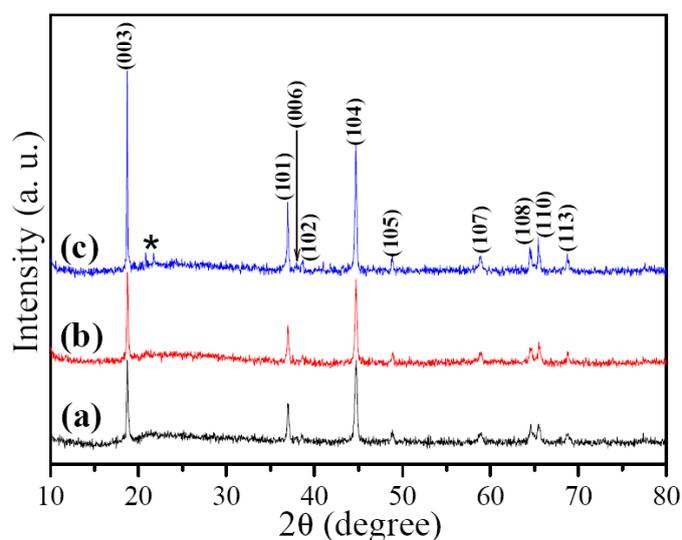


**Figure 1.** XRD patterns of $Li_{1.2}Ni_{0.13}Co_{0.13}Mn_{0.54}O_2$ obtained at different calcination temperatures: (a) 750, (b) 850 and (c) 950$^o$C, and the asterisk-marked peak can be attributed to the superlattice ordering characteristics for the periodic occupation of Li ions in the transition metal layers of a $LiMO_2$

It has been well proved that the calcination temperature is essential for the formation of $Li_{1.2}Ni_{0.13}Co_{0.13}Mn_{0.54}O_2$ [22, 27, 31]. Thus, the influence of calcination temperature is considered firstly. Fig. 1 shows the XRD patterns of serial $Li_{1.2}Ni_{0.13}Co_{0.13}Mn_{0.54}O_2$ samples obtained at different temperatures. The each diffraction peak of which can be indexed those of crystalline α-NaFeO$_2$. XRD pattern of each target sample is consistent with the standard data of the crystal structure of layered LiMO$_2$. Also, the asterisk-marked weak diffraction peaks in the 2θ range of 20$^o$ and 25$^o$ can be ascribed to the XRD characteristics for the partial occupation of Li$^+$ ions in the transition metal layers of crystalline LiMO$_2$, suggesting the existence of crystalline Li$_2$MnO$_3$ (also called as layered Li(Li$_{1/3}$Mn$_{2/3}$)O$_2$) component [8-14]. Besides, with the increased calcination temperatures, the improved peak intensity and elevated intensity ratio of (003) to (104) ($I_{(003)}/I_{(104)}$) (i.e., peak height ratio) can be clearly observed in Fig. 1 and Tab. 1, indicating the elevated calcination temperature should be helpful for improving the crystallinity and layered structures [22, 27]. Furthermore, the actual element composition of $Li_{1.2}Ni_{0.13}Co_{0.13}Mn_{0.54}O_2$ obtained at 850$^o$C also has been tested by ICP-AES, as shown in Tab. 2. The chemical formula of 850$^o$C sample also can be denoted as $Li_{1.165}Ni_{0.130}Co_{0.136}Mn_{0.532}O_2$ by this test. This result is close to the addition of raw materials. As for 750 or 900$^o$C sample, the ratio of Ni, Co and Mn should be consistent with 850$^o$C sample.

**Table 1.** Lattice parameters, $I_{(003)}/I_{(104)}$ ratios and FWHM$_{(003)}$ values of serial $Li_{1.2}Ni_{0.13}Co_{0.13}Mn_{0.54}O_2$ estimated from XRD data and space group R-$\bar{3}$m.

| Temperature ($^o$C) | a (Å) | c (Å) | $I_{(003)}/I_{(104)}$ | FWHM$_{(003)}$ | Size (nm) |
|---|---|---|---|---|---|
| 750 | 2.842 | 14.165 | 1.04 | 0.179 | 49.97 |
| 850 | 2.845 | 14.210 | 1.21 | 0.164 | 54.55 |
| 950 | 2.846 | 14.220 | 1.58 | 0.106 | 84.40 |
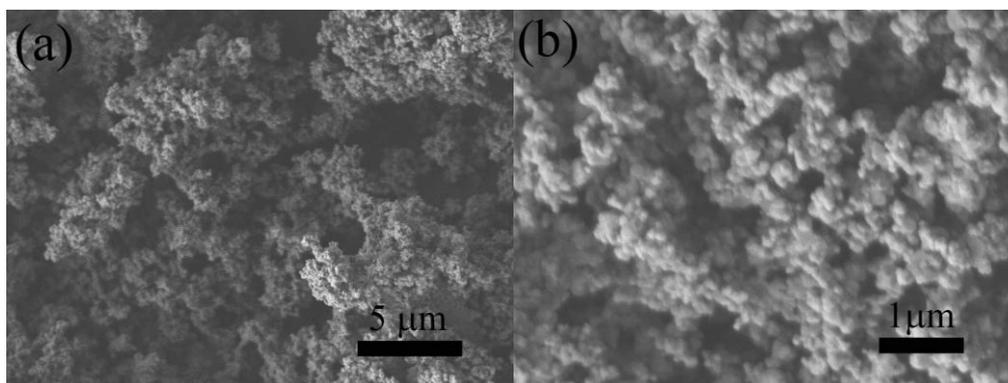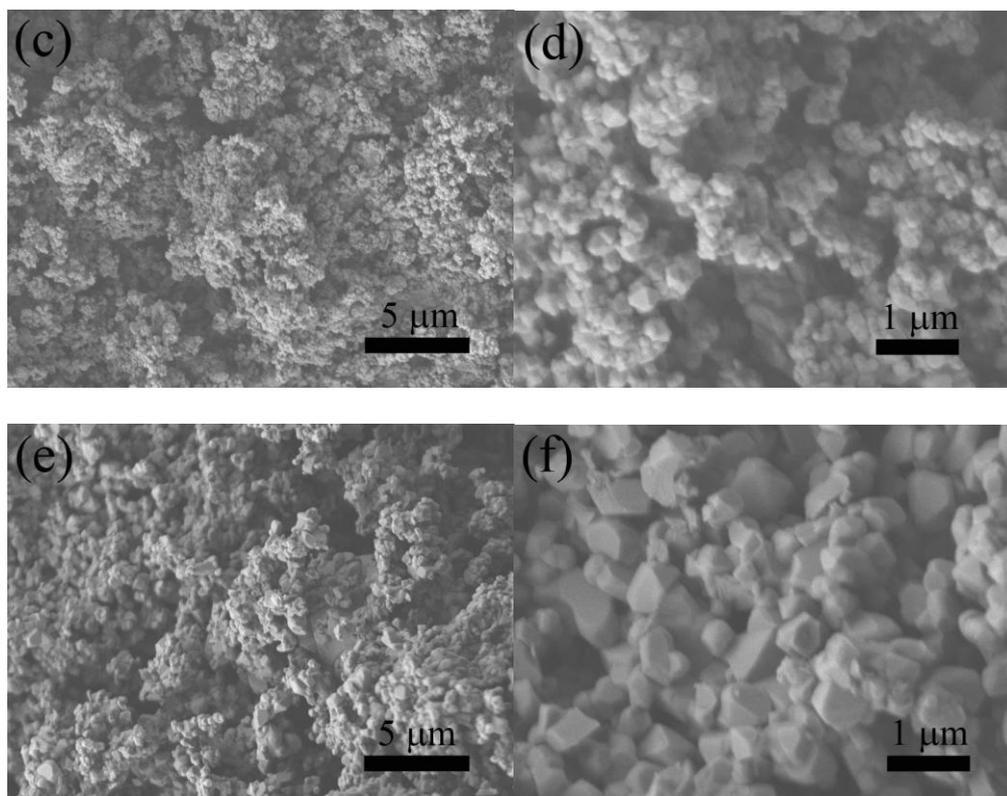
**Figure 2.** SEM images of $Li_{1.2}Ni_{0.13}Co_{0.13}Mn_{0.54}O_2$ obtained from different calcination temperatures: (a, b) 750, (c, d) 850 and (e, f) 950°C

Fig. 2 reveals the SEM images of $Li_{1.2}Ni_{0.13}Co_{0.13}Mn_{0.54}O_2$ obtained from different crystallization temperatures. These samples are made up of numerous polyhedral nanoparticles, and parts of them show sharp edges and smooth facets (Fig. 2 d and f), indicating that they are well constructed. With the elevated calcination temperature, the particle size increases form ~100 nm (750°C) to 500-700 nm (950°C), and the sample has a moderate size of ~200 nm at 850°C.

**Table 2.** The actual element composition of $Li_{1.2}Ni_{0.13}Co_{0.13}Mn_{0.54}O_2$ obtained at 850°C detected by ICP-AES

| Element | Li | Ni | Co | Mn |
|---------|------|------|------|------|
| Ratio | 8.95 | 1.00 | 1.05 | 4.09 |

This change is consistent with estimated size from XRD patterns (Tab. 2), which base on the $FWHM_{(003)}$ (Full Width Half Maximum of (003) crystal plane) values and Scherrer equation ($D = k\lambda/\cos\theta$)。
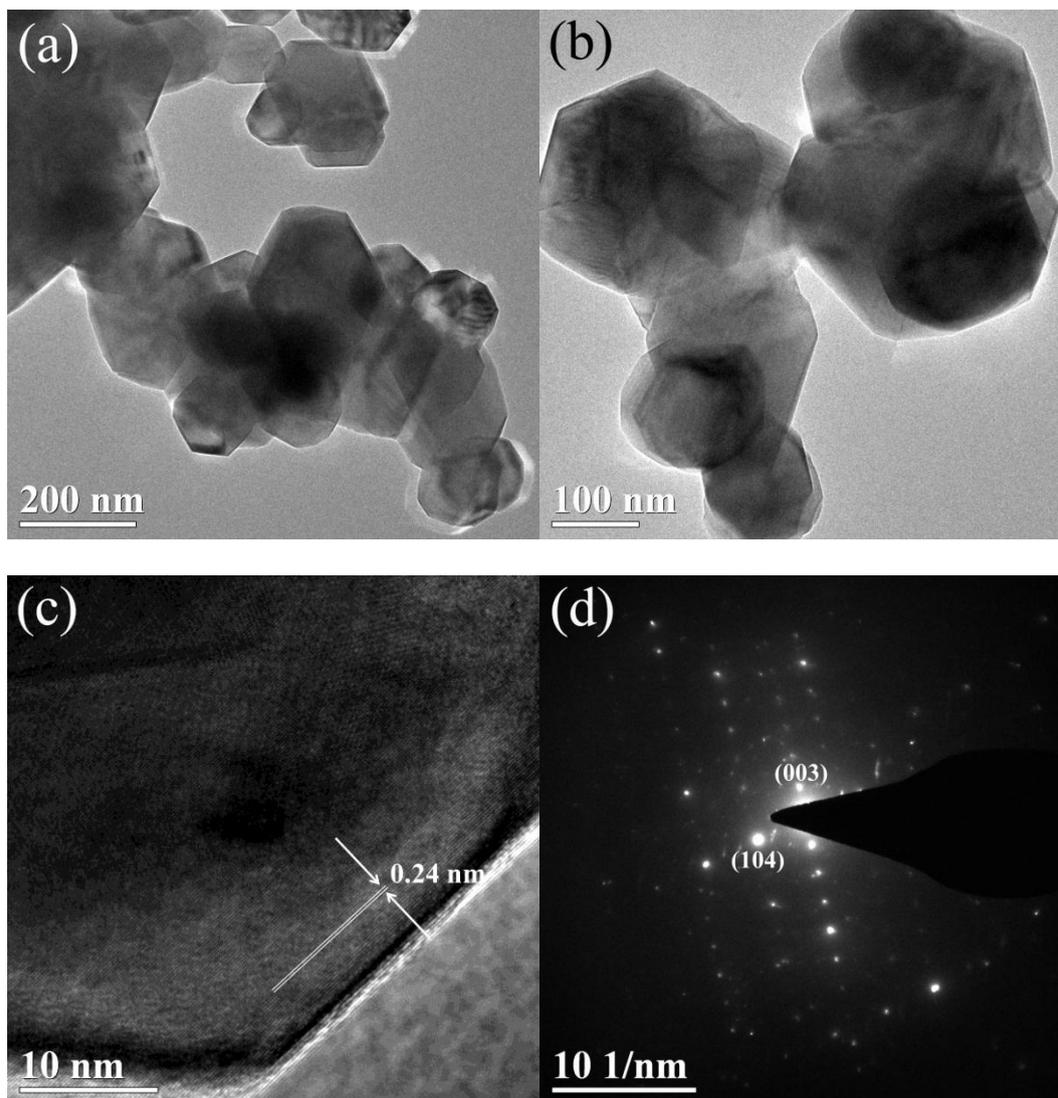
**Figure 3.** (a, b) TEM, (c) HR-TEM image and (d) selected area electron diffraction (SAED) pattern of $Li_{1.2}Ni_{0.13}Co_{0.13}Mn_{0.54}O_2$ nanoparticles obtained at $850^oC$

To further investigate the structures and morphologies of as-prepared sample, Fig. 3 reveals the TEM, HR-TEM image and SAED pattern of $Li_{1.2}Ni_{0.13}Co_{0.13}Mn_{0.54}O_2$ sample obtained at $850^oC$. The morphologies in TEM image (Fig. 3a and b) are consistent with SEM image, and these nanoparticles have the size of ~200 nm. In Fig. 3c, the lattice distance of 0.24 nm can be indexed to the (104) crystal face of lithium rich layered oxides. The SAED pattern (Fig. 3d) shows the polycrystalline nature of these random nanoparticles. Furthermore, some diffraction dots such as (003) and (104) peak can be clearly detected, which can be indexed to the XRD pattern in Fig. 1.

As lithium ion battery cathodes, it is accepted that: (i) the improved layered structure and good crystallinity of electrode materials can provide stable framework during cycling and then elevate its cycling stability; (ii) the enlargement of particle size may inhibit the effective diffusion of lithium ions and electrons within the interface and inner of material.
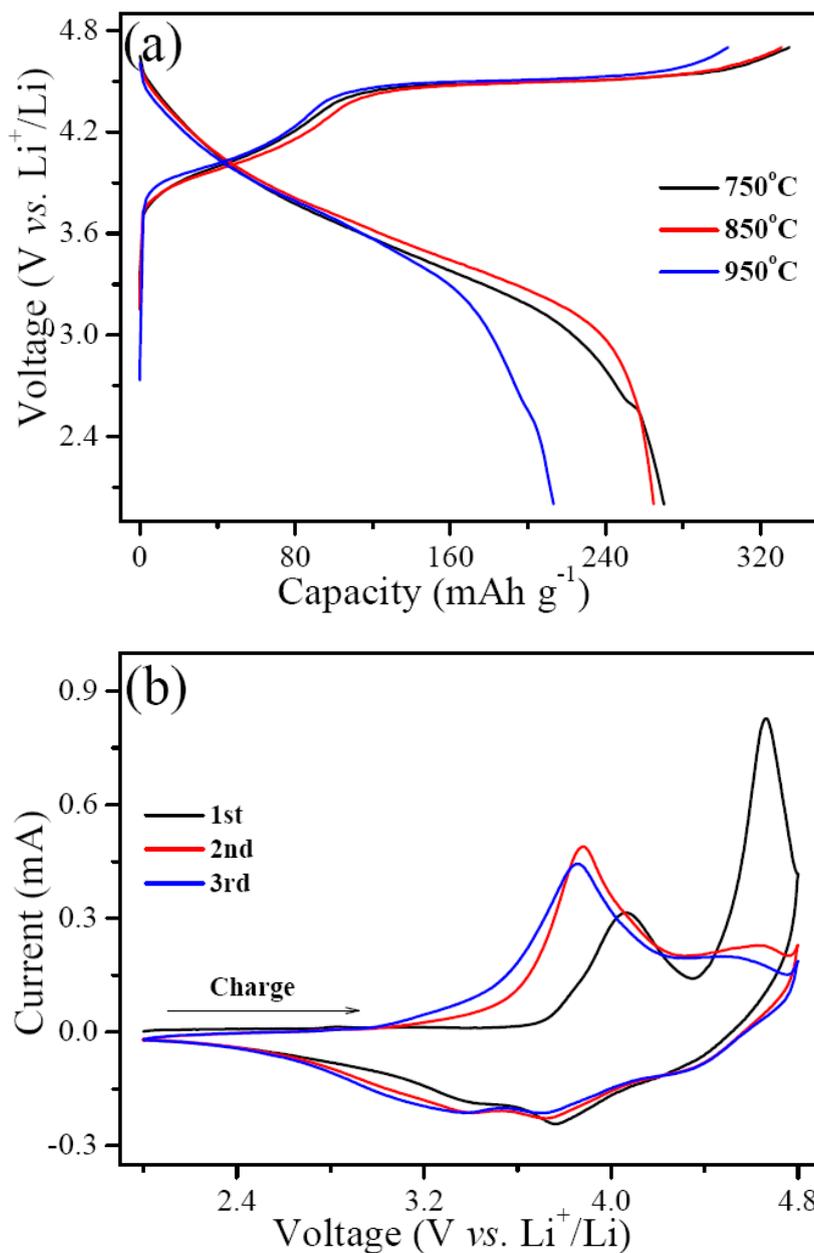
**Figure 4.** (a) Initial charge discharge curves of $Li_{1.2}Ni_{0.13}Co_{0.13}Mn_{0.54}O_2$ obtained at different calcination temperatures recorded at 20 mA g$^{-1}$ within 2.0-4.7 V and (b) CV profiles of the three first cycles of $Li_{1.2}Ni_{0.13}Co_{0.13}Mn_{0.54}O_2$ obtained at 850°C recorded at 0.1 mV s$^{-1}$ within 2.0-4.8 V

Thus, the electrochemical performances of obtained $Li_{1.2}Ni_{0.13}Co_{0.13}Mn_{0.54}O_2$ will be determined by their structural parameters. Fig. 4a reveals initial charge-discharge profiles of $Li_{1.2}Ni_{0.13}Co_{0.13}Mn_{0.54}O_2$/Li cells recorded at a low current density of 20 mA g$^{-1}$ within 2.0 and 4.7 V (*vs.* Li$^+$/Li). At a calcination temperature of 750, 850 or 950°C, the resulting $Li_{1.2}Ni_{0.13}Co_{0.13}Mn_{0.54}O_2$ sample gives a specific discharge capacity of 270.2, 264.9 or 213.2 mAh g$^{-1}$ accompanying with a coulombic efficiency of 80.7%, 80.1% or 70.3%, respectively. Apprantly, the low temperature samples (750 and 850°C) have higher discharge capacity and Coulombic effeciency, which should benefit from their smaller particle sizes. Fig. 4b shows the CV curves of 850°C $Li_{1.2}Ni_{0.13}Co_{0.13}Mn_{0.54}O_2$ electrode

for the initial three cycles. During the first charge process, an anodic peak at ~4.05 V can be attributed to the de-intercalation of Li ions from $LiNi_{1/3}Co_{1/3}Mn_{1/3}O_2$ phase with the oxidation of $Ni^{2+}$ ions. A sharp oxidation peak nearby 4.6 V corresponds to the transformation of $Li_2MnO_3$ into layered $MnO_2$ and the oxidation of $Co^{3+}$ ions. In the initial discharge process, the wide cathodic peak located 3.4-3.8 V indicates the intercalation of $Li^+$ ions into layered $Ni_{1/3}Co_{1/3}Mn_{1/3}O_2$ and $MnO_2$ [10, 24]. In the subsequent cycles (i.e., 2$^{nd}$ and 3$^{rd}$ cycle), the continuous oxidation-reduction of layered $LiNi_{1/3}Co_{1/3}Mn_{1/3}O_2$ and $LiMnO_2$ result in the stable peak current, as shown in Fig. 4b.
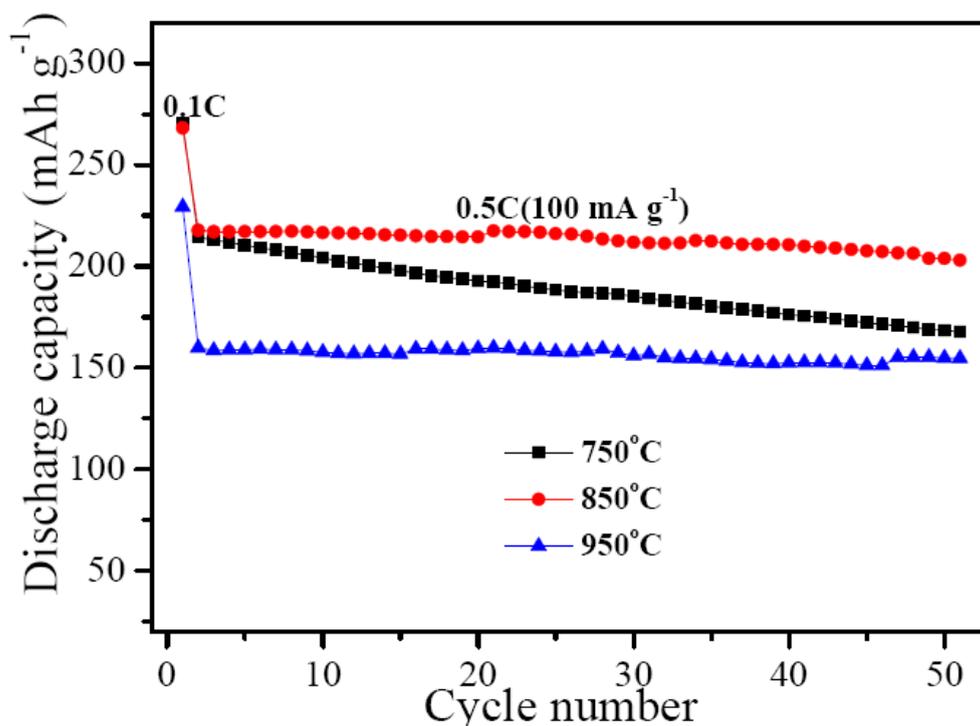


**Figure 5.** Cycling performances of different $Li_{1.2}Ni_{0.13}Co_{0.13}Mn_{0.54}O_2$ samples

Besides the discharge capcity, the cycling stability is key for electrode materials. After initial activation of $Li_2MnO_3$ at 20 mA g$^{-1}$, the cycling stability of different $Li_{1.2}Ni_{0.13}Co_{0.13}Mn_{0.54}O_2$ are recorded at 100 mA g$^{-1}$. As shown in Fig. 5, the 2$^{nd}$ specific discharge capacities of $Li_{1.2}Ni_{0.13}Co_{0.13}Mn_{0.54}O_2$ series obtained from 750, 850 and 950$^o$C are 214.4, 217.8 and 159.7 mAh g$^{-1}$ at 100 mA g$^{-1}$. Until 50 cycles, the residual values are 167.7, 203.0, and 154.7 mAh g$^{-1}$, accordingly giving a retention ratio of 78.2%, 93.2% and 96.9%. Apparently, the elevated synthesis temperature can effectively improve the cycling stability of $Li_{1.2}Ni_{0.13}Co_{0.13}Mn_{0.54}O_2$, and the improved cycling stability with elevated calcination temperature can be attributed to the enhanced layered structure. It also can be determined that the 850$^o$C sample has optimal electrochemical performances based on its high discharge capacity and good cycling performance.
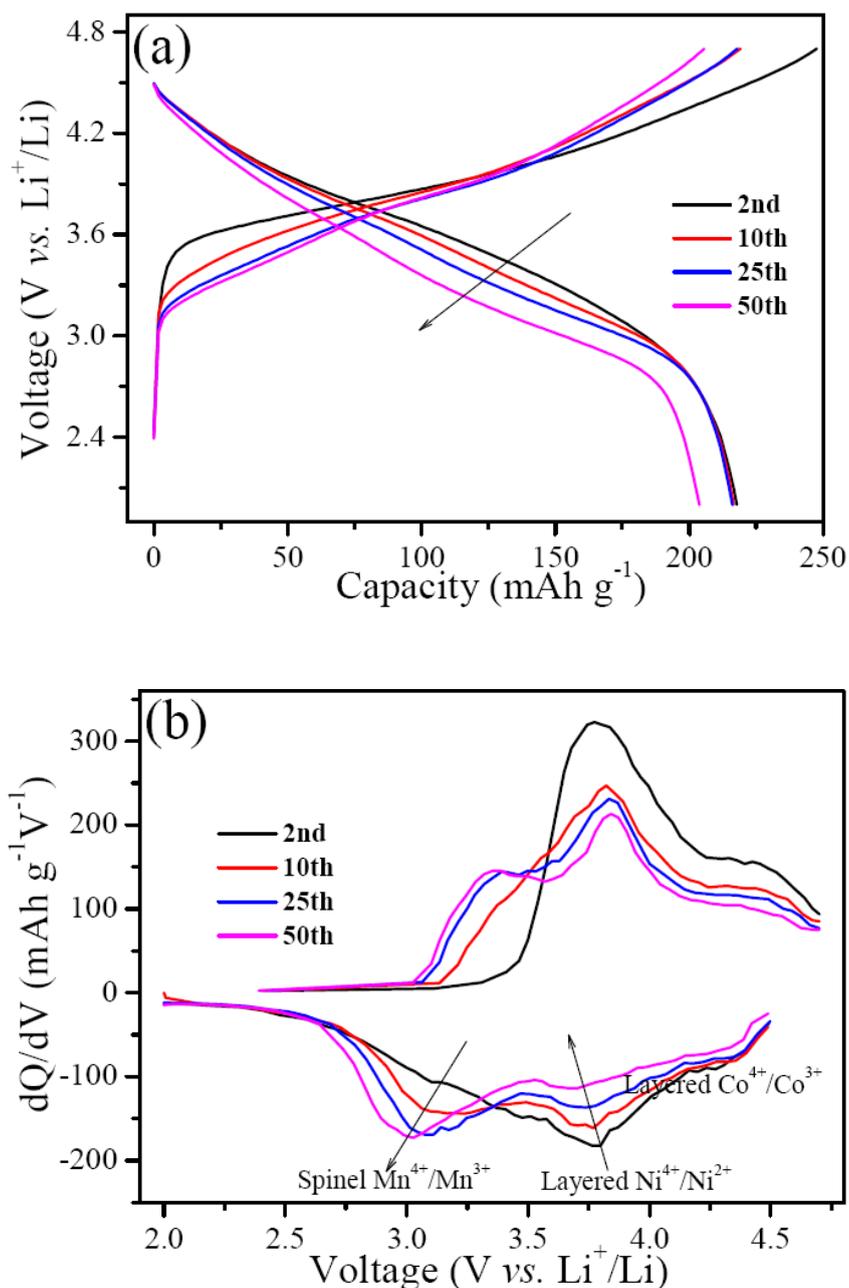
**Figure 6.** (a) Typical $2^{nd}$, $10^{th}$, $25^{th}$ and $50^{th}$ charge-discharge profiles and (b) corresponding dQ/dV curves of $850^{o}C$ $Li_{1.2}Ni_{0.13}Co_{0.13}Mn_{0.54}O_2$ sample

In order to study the capacity and voltage decay upon cycling, typical $2^{nd}$, $10^{th}$, $25^{th}$ and $50^{th}$ charge-discharge curves and corresponding dQ/dV curves of $850^{o}C$ $Li_{1.2}Ni_{0.13}Co_{0.13}Mn_{0.54}O_2$ sample are showed in Fig. 6. All electrode experience a gradual decay of discharge voltage with increased cycles (Figure 6a), and this is due to a combined potential shift of the layered $Co^{4+}/Co^{3+}$, $Ni^{4+}/Ni^{2+}$, and spinel $Mn^{4+}/Mn^{3+}$ peaks along with the galvanostatic cycles (Fig. 6b). As the cycle number increases, the cathodic peak of the layered $Ni^{4+}/Ni^{2+}$ nearby 3.8 V weakens gradually, and the cathodic peak of the spinel $Mn^{4+}/Mn^{3+}$ nearby 3.0 V increases step by step, indicating a continuous phase transformation from layered $LiMnO_2$ to spinel $LiMn_2O_4$ [25, 32]. Maybe, it's necessary to inhibit the voltage decay of lithium rich layered oxides by ions doping and/or surface modification [6, 7].
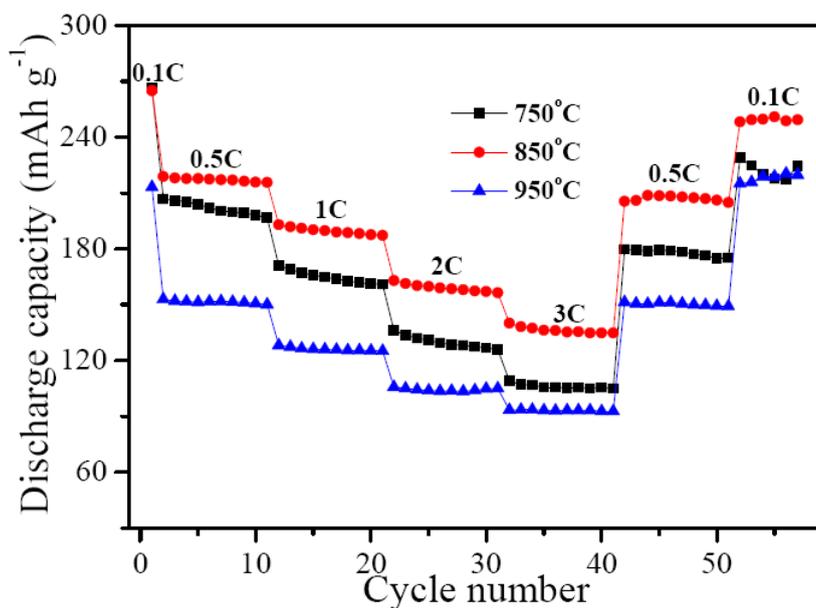
**Figure 7.** Discharge capacity and cycling performances of various $Li_{1.2}Ni_{0.13}Co_{0.13}Mn_{0.54}O_2$ at various current densities

The rate capability of series $Li_{1.2}Ni_{0.13}Co_{0.13}Mn_{0.54}O_2$ electrodes is revealed in Fig. 7. It is shown that, after the initial activation of $Li_2MnO_3$ at the 1st cycle, the specific capacity value of each sample gradually decreases with the increasing current density from 0.5 to 3C (600 mA $g^{-1}$).
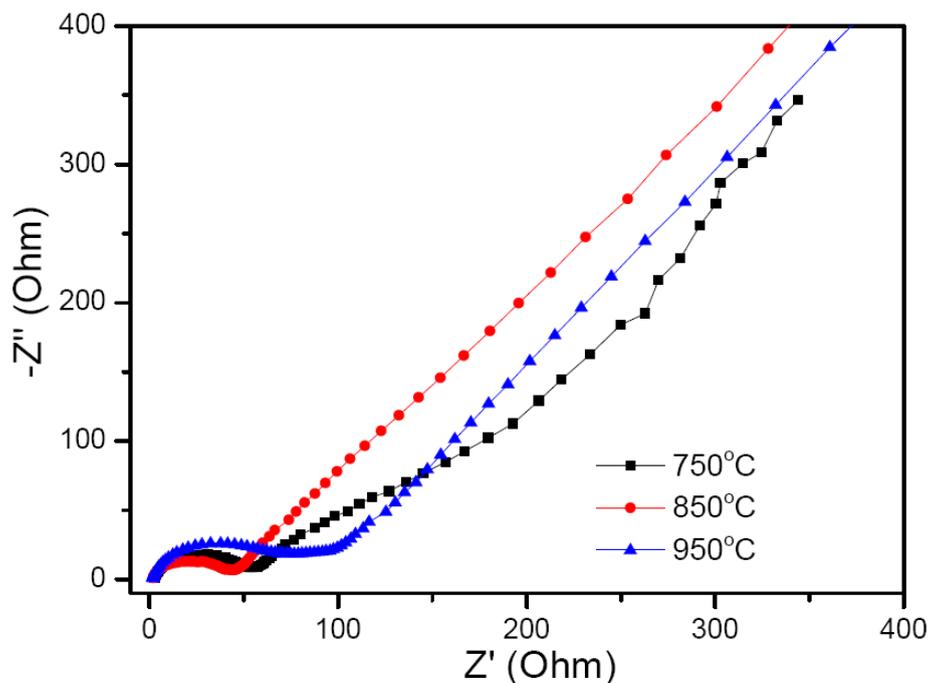


**Figure 8.** EIS results of fresh different $Li_{1.2}Ni_{0.13}Co_{0.13}Mn_{0.54}O_2$ electrodes recorded at an electrochemical workstation (CHI660, Shanghai) with a frequency ranges 0.1 MHz to 0.01 Hz and voltage of 3.7 V.

In detail, the 22$^{nd}$ specific discharge capacity is 136.1 (750$^{o}$C), 163.0 (850$^{o}$C) or 105.8 (950$^{o}$C) mAh g$^{-1}$ at 2C, and the 32$^{nd}$ reversible capacity (3C) still keeps at a value of 109.0 (750$^{o}$C), 140.1 (850$^{o}$C) or 93.3 (950$^{o}$C) mAh g$^{-1}$. Importantly, when the current density goes back to 0.1C, the 52$^{nd}$ cycle discharge capacity returns to a high value of 228.8 (750$^{o}$C), 248.3 (850$^{o}$C) or 215.1 (950$^{o}$C) mAh g$^{-1}$ (Fig. 7). Furthermore, a comparative capacity ratios of 3C (32$^{nd}$ cycle) to 0.1C (52$^{nd}$ cycle) is 47.6%, 56.4% or 43.3%, respectively. These indicate that, the 850$^{o}$C sample has best rate capability comparing with other two samples, and its high discharge capacity at current density of 3C should be suitable for high-rate lithium ion battery application.

Electrochemical conductivity of three different samples is also studied by Electrochemical Impedance Spectroscope (EIS), as shown in Fig. 8. All the Nyquist plots show a high-frequency semicircle and a low-frequency slope line, corresponding to an electrolyte-electrode interfacial resistance of charge transfer ($R_{ct}$) and a Warburg impedance of lithium diffusion within the electrode, respectively. The working electrode possesses an approximate $R_{ct}$ value of 41.43, 29.52 and 59.22 $\Omega$ for 750, 850 and 950$^{o}$C sample, respectively. This variation is close to the high-rate cycling stability in Fig. 7.

# 4. CONCLUSION

Herein, we develop a facile eutectic acetate route to prepare high-capacity lithium ion battery cathode $Li_{1.2}Ni_{0.13}Co_{0.13}Mn_{0.54}O_2$. The influences of calcination temperature on the structure and electrochemical performances are comparatively studied. At the optimal temperature of 850$^{o}$C, the resulting nanoparticles with the size of ~200 nm present clear edge and corner. As lithium ion battery cathode, the sample shows an initial discharge capacity of 264.9 mAh g$^{-1}$ with Coulombic efficiency of 80.1% at 20 mA g$^{-1}$ and retains a discharge capacity of 203.0 mAh g$^{-1}$ at 100 mA g$^{-1}$ after 50 cycles. Maybe, the $Li_{1.2}Ni_{0.13}Co_{0.13}Mn_{0.54}O_2$ obtained from simple and green eutectic acetate route is suitable for lithium ion battery application, deserved to be conducted continuously.

## References

1.  B. L. Ellis, K. T. Lee, L. F. Nazar, *Chem. Mater*, 22 (2010) 691
2.  J. B. Goodenough, Y. S. Kim, *Chem. Mater*, 22 (2010) 587
3.  M. Hu, X. L. Pang, Z. Zhou, *J. Power Sources*, 237 (2013) 229
4.  M. M. Thackeray, C. S. Johnson, J. T. Vaughey, N. Li, S. A. Hackney, *J. Mater. Chem*, 15 (2005) 2257

5.  M. M. Thackeray, S. H. Kang, C. S. Johnson, J. T. Vaughey, R. Benedek, S. A. Hackney, *J. Mater. Chem*, 17 (2007) 3112
6.  P. He, H. J. Yu, H. S. Zhou, J. *Mater. Chem*, 22 (2012) 3680
7.  H. J. Yu, H. S. Zhou, *J. Phys. Chem. Lett*, 4 (2013) 1268
8.  J. Gao, Z. L. Huang, J. J. Li, X. X. He, C. Y. Jiang, *Ionics*, 20 (2014) 301
9.  H. J. Yu, R. Ishikawa, Y. G. So, N. Shibata, T. Kudo, H. S. Zhou, Y. Ikuhara, *Angew. Chem. Int*. Edit, 52 (2013) 5969
10. C. H. Zhao, X. X. Wang, X. R. Liu, H. Zhang, Q. Shen, *ACS. Appl. Mater. Inter*, 6 (2014) 2386
11. S. Kim, C. Kim, Y. I. Jhon, J. K. Noh, S. H. Vemuri, R. Smith, K. Y. Chung, M. S. Jhon, B. W. Cho, J. *Mater. Chem*, 22 (2012) 25418
12. C. H. Zhao, X. X. Wang, R. Liu, X. R. Liu, Q. Shen, *Ionics*, 20 (2014) 645
13. C. S. Johnson, N. C. Li, C. Lefief, J. T. Vaughey, M. M. Thackeray, *Chem. Mater*, 20 (2008) 6095
14. X. J. Guo, Y. X. Li, M. Zheng, J. M. Zheng, J. Li, Z. L. Gong, Y. Yang, *J. Power. Sources*, 184 (2008) 414
15. O. Toprakci, H. A. K. Toprakci, Y. Li, L. W. Ji, L. G. Xue, X. W. Zhang, *J. Power. Sources*, 241 (2013) 522
16. K. C. Jiang, X. L. Wu, Y. X. Yin, J. S. Lee, J. Kim, Y. G. Guo, *ACS. Appl. Mater. Inter*, 4 (2012) 4858
17. J. H. Lim, H. J. Bang, K. S. Lee, K. Amine, Y. K. Sun, *J. Power. Sources*, 189 (2009) 571
18. L. J. Zhang, B. R. Wu, N. Li, F. Wu, *Electrochim. Acta*, 118 (2014) 67
19. Y. Chen, G. F. Xu, J. L. Li, Y. K. Zhang, Z. Chen, F. Y. Kang, *Electrochim. Acta*, 87 (2014) 686
20. J. B. Li, Y. L. Xu, X. F. Li, Z. W. Zhang, *Appl. Surf. Sci*, 285P (2013) 235
21. J. M. Zheng, X. B. Wu, Y. Yang, *Electrochim. Acta*, 56 (2011) 3071
22. J. L. Liu, L Chen, M. Y. Hou, F Wang, R. C. Che, Y. Y. Xia, *J. Mater. Chem*, 22 (2012) 25380
23. S. J. Shi, J. P. Tu, Y. Y. Tang, X. Y. Liu, X. Y. Zhao, X. L. Wang, C. D. Gu, *J.Power Sources*, 241 (2013) 186
24. C. H. Zhao, W. P. Kang, R. Liu, Q. Shen, *RSC. Adv*, 2 (2013) 2362
25. T. L. Zhao, S. Chen, L. Li, X. F. Zhang, R. J. Chen, I. Belharouak, F. Wu, K. Amine, *J. Power. Sources*, 228 (2013) 206
26. D. Luo, G. S. Li, X. F. Guan, C. Yu, J. Zheng, X. H. Zhang, L. P. Li, *J. Mater. Chem*. A, 1 (2013) 1220
27. D. Luo, G. S. Li, C. C. Fu, J. Zheng, J. M. Fan, Q. Li, L. P. Li, *Adv. Energy. Mater*, 4 (2014) 1
28. X. Feng, Y. Lu, N. Ding, X. Y. Feng, C. Liu, C. H. Chen, *Electrochim. Acta*, 55 (2010) 832
29. U. Lafont, C. Locati, E. M. Kelder, *Solid. State. Ionics*, 177, (2006) 3023
30. G. Du, Y. Nuli, J. Yang, J. Wang, *Mater. Res. Bull*, 43 (2008) 3607
31. W. C. West, J. Soler, B. V. Ratnakumar, *J. Power. Sources*, 204 (2012) 200
32. B. H. Song, Z. W. Liu, M. O. Lan, L. Lu, *Phys. Chem. Chem. Phys*, 14 (2012) 12875